JTE HCMUTE
ISSN: 2615-9740

JOURNAL OF TECHNICAL EDUCATION SCIENCE
Ho Chi Minh City University of Technology and Education
Website: https://jte.hcmute.edu.vn/index.php/jte/index
Email: jte@hcmute.edu.vn

A Novel Least-Squares Level Set Method by Using Polygonal Elements

Ba-Dinh Nguyen-Tran[1], Son H. Nguyen[2], Duc-Huynh Phan[3*]

[1]*Japan Technology and Engineering Co. Ltd, Viet Nam*
[2]*Ton Duc Thang University, Ho Chi Minh City, Viet Nam*
[4]*Faculty of Civil Engineering, Ho Chi Minh City University of Technology and Education, Viet Nam*

[*] Corresponding author. *Email: huynhpd@hcmute.edu.vn*

ARTICLE INFO

Received: 22/06/2022
Revised: 08/08/2022
Accepted: 27/09/2022
Published: 28/10/2022

KEYWORDS

Polygonal Elements;
Level Set Method;
Convection-diffusion;
Least-squares method;
Re-initialization.

ABSTRACT

In this study, we apply an artificial viscosity method to convert an unsteady level set (LS) convection equation into an unsteady LS convection-diffusion transport equation to stabilize the numerical solution of the convection term. Then a novel least-square polygonal finite element method is used to solve an unsteady LS convection-diffusion problem. The least-squares method provided good mathematical properties such as natural numerical diffusion and the positive definite symmetry of the resulting algebraic systems for the convection-diffusion and re-initialization equations. The proposed method is evaluated numerically in two different benchmark problems: a rigid body rotation of Zalesak's disk, and a time-reversed single-vortex flow. In comparison with conventional triangular (T3) and quadrilateral (Q4) elements, polygonal elements are capable of providing greater flexibility in mesh generation for complicated problems as well as more accurate in solving the LS equations. In addition, the numerical results are also compared with the results which obtained from essentially non-oscillatory type formulations and particle LS methods. The results show that the proposed method completely matches the previously published results.

Doi: https://doi.org/10.54644/jte.72A.2022.1232

1. Introduction

Level set method (LSM) the most common method for numerical simulation of moving interfaces and is increasingly expanding into many engineering fields because of its good properties. The basic idea of this method is solving an unsteady LS convection equation for an auxiliary function ϕ whose zero level set defines the shape of the free interface [1], [2]. However, solving this equation often gives the result that has the oscillation of the solution (weak solution) caused by the convection term. To solve this issue, Osher and Fedkim (2003) [3] proposed an artificial viscosity method which was performed by adding an artificial diffusion term into the right-hand side of the unsteady LS convection equation. Their results show that artificial diffusion term is effective in eliminating the oscillation of the solution.

In a typical process, the solution of LS equation is usually initialized by a signed distance function (SDF) satisfying the Eikonal equation, i.e. $|\nabla\phi| = 1$ [2]. In moving process of interface, the SDF property is generally lost and causes the LS function to become too flat or too steep. This problem can be solved by using the re-initialization techniques [4] – [7]. Sussman et al. (1994) [4] presented a re-initialization method in which a hyperbolic partial differential equation (PDE) is solved to steady state. Their results show that one needs to re-initialize after every time step in order to keep the solution accurate. However, this method leads to significant displacements of the interface, and the time reaches steady state is too long. Elias et al. (2007) [7] proposed a new method for computing distance functions in unstructured grids imposing the satisfaction of Eikonal equation at element level. This method is easy to implement and can be readily employed in finite element solvers since all information necessary is available or is readily built as derived data structures.

Note that most of the above studies are all focused on T3 and Q4 elements to solve the 2D problems. Meanwhile, both these elements have certain advantages and disadvantages. T3 elements are suitable

JTE
HCMUTE
ISSN: 2615-9740

JOURNAL OF TECHNICAL EDUCATION SCIENCE
Ho Chi Minh City University of Technology and Education
Website: https://jte.hcmute.edu.vn/index.php/jte/index
Email: jte@hcmute.edu.vn

for forming mesh with complex geometries, but its accuracy and solution convergence are low. On the contrary, the accuracy and solution convergence of Q4 elements are high, but its meshing ability is difficult. In recent years, polygonal finite elements with a lot of good features have been widely applied in mechanics problems. However, using it into LSM is still limited. Compared to T3 and Q4 elements, polygonal elements are capable of providing greater flexibility in mesh generation for complicated problems and are sometimes more accurate and provide robust results [8], [9].

In the finite element method (FEM) framework for LSM, using the standard Galerkin method to discrete spatial domain is the simplest and most common method. However, this method will give oscillating solutions [5]. Therefore, many previously researches have been introduced to obtain a stable FE solution such as streamline-upwind Petrov-Galerkin (SUPG) [10], characteristic Galerkin [11], discontinuous Galerkin [12], Taylor-Galerkin (TG) [13], and standard least-squares [3], [5]. However, the most literatures are limited for T3 and Q4 elements.

In the present study, we also apply the standard least-squares method [3], [5] to solve the LS equation. It is different here that we are not only limited to use the T3 and Q4 elements, but also extend to the polygonal elements. The effectiveness of this method is investigated by some benchmark problems. This paper is organized as follows. The next section presents the theory of the conventional level set evolution (LSE) method. Section 3 focuses on the formulation of the polygonal finite element method (Poly-FEM) for level set evolution. The numerical results are presented and discussed in Section 4. Finally, some conclusions are drawn in Section 5.

2. Conventional level set evolution

2.1. Implicit level set representation

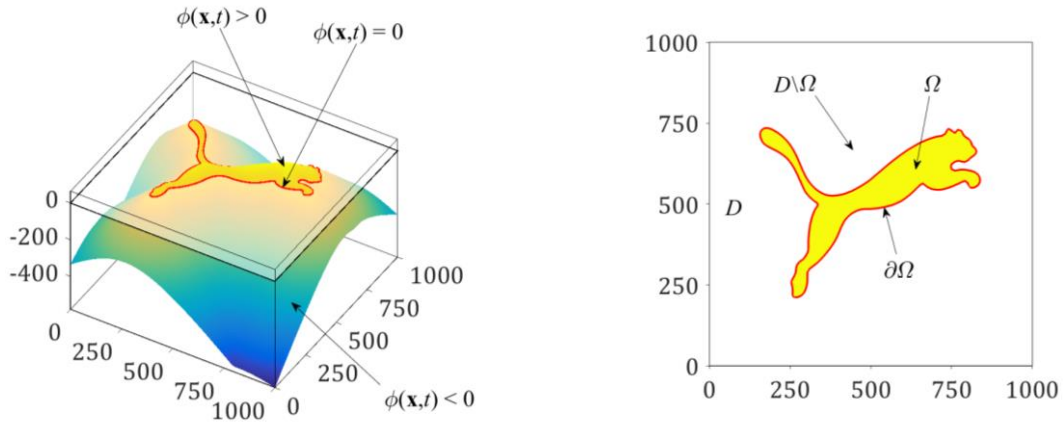

(a) *(b)*

Figure 1. *Level set description of a two-dimensional design: (a) Level set model; (b) Computational domain*

In the LSM [5], we consider a moving interface $\partial\Omega$ which implicitly represented by the zero value of the LS function $\phi(\boldsymbol{x})$, i.e. $\partial\Omega = \{\forall \boldsymbol{x} \in \mathcal{D} : \phi(\boldsymbol{x}) = 0\}$. Therein, $\mathcal{D} \subset \mathbb{R}^2$ is a computational domain containing a subdomain Ω so that $\Omega \subset \mathcal{D}$. The LS function illustrated in Figure 1 and has the following properties:

$$\begin{cases} \phi(\boldsymbol{x}) < 0 \Leftrightarrow \forall \boldsymbol{x} \in \Omega\backslash\partial\Omega \\ \phi(\boldsymbol{x}) = 0 \Leftrightarrow \forall \boldsymbol{x} \in \partial\Omega \\ \phi(\boldsymbol{x}) > 0 \Leftrightarrow \forall \boldsymbol{x} \in \mathcal{D}\backslash(\Omega \cup \partial\Omega) \end{cases} \tag{1}$$

In Eq. (1), Ω is a region bounded by the moving interface $\partial\Omega$. The evolution of this interface is specified by solving an unsteady LS convection equation [1]

$$\forall \boldsymbol{x} \in \mathcal{D}, \quad \frac{\partial \phi}{\partial t} - (\boldsymbol{v} \cdot \nabla)\phi = 0 \quad \text{with} \quad \phi(\boldsymbol{x}, 0) = \phi_0(\boldsymbol{x}) \tag{2}$$

where $\phi_0(\boldsymbol{x})$ is an initial LS function and it contains signed SDF property, i.e. $|\nabla\phi_0(\boldsymbol{x})| \cong 1$; t is the pseudo time variable; $\boldsymbol{v} = \boldsymbol{v}(\boldsymbol{x}, t)$ is the velocity field. In order to stabilize the numerical solution of

the convection term $(\boldsymbol{v}\cdot\nabla)\phi$ in Eq. (2), an artificial viscosity (diffusion) term $\nabla\cdot(\varepsilon\nabla\phi)$ is generally added to the right-hand side of Eq. (2) [3], where ε is a very small viscosity coefficient. In summary, the LS equation (2) can be rewritten as an unsteady LS convection-diffusion transport equation:

$$\frac{\partial\phi}{\partial t}+(\boldsymbol{v}\cdot\nabla)\phi-\nabla\cdot(\varepsilon\nabla\phi)=0 \qquad \text{in } \mathcal{D}\times\mathcal{T} \tag{3}$$

$$\phi(\boldsymbol{x},0)=\phi_0(\boldsymbol{x}) \qquad \text{in } \mathcal{D}\times\{0\} \tag{4}$$

where $\mathcal{T}$ is an interval time for the evolution of the LS function. Since $\mathcal{T}$ is chosen to be a small interval time between two iterations of evolutional process, the convection velocity in (3) is assumed to be independent over $\mathcal{T}$, i.e. $\boldsymbol{v}(\boldsymbol{x},t)\approx\boldsymbol{v}(\boldsymbol{x},0)=:\boldsymbol{v}(\boldsymbol{x})$. Consequently, the unsteady LS convection-diffusion problem (3) becomes a linear convection problem.

2.2. Level set re-initialization process

During the process of the interface evolution, the LS function may become too steep or too flat near the interface because of cumulative error. To solve this problem, a re-initialization process should be applied to maintain the SDF feature of LS function by solving an Eikonal equation [3] – [5]. In order to stabilize the numerical solution of the convection term in the Eikonal equation, the artificial viscosity method is also applied. Therefore, we have:

$$\frac{\partial\psi}{\partial\tau}+(\boldsymbol{c}\cdot\nabla)\psi-\nabla\cdot(\varepsilon\nabla\psi)=\mathcal{s}(\phi) \qquad \text{in } \mathcal{D}\times\mathcal{T}_\tau \tag{5}$$

$$\psi(\boldsymbol{x},0)=\phi(\boldsymbol{x}) \qquad \text{in } \mathcal{D}\times\{0\} \tag{6}$$

where τ is the virtual time variable, $\mathcal{T}_\tau$ is a virtual interval time of the re-initialization process, $\psi=\psi(\boldsymbol{x},\tau)$ is a corrected LS function, $\boldsymbol{c}(\phi;\boldsymbol{x},\tau):=\mathcal{s}(\phi)\boldsymbol{n}(\boldsymbol{x},\tau)$ is the characteristic velocity with $\boldsymbol{n}(\boldsymbol{x},t)=\frac{\nabla\psi(\boldsymbol{x},\tau)}{\max(10^{-8},|\nabla\psi(\boldsymbol{x},\tau)|)}$ is the unit outward normal vector, $\mathcal{s}(\phi):=\frac{\phi}{\sqrt{\phi^2+\varrho^2}}$ is smoothed sign function, and $\varrho=2h$ is the size of the smoothing zone (h is the element size). Eq. (5) is a nonlinear problem because the characteristic velocity $\boldsymbol{c}(\phi;\boldsymbol{x},\tau)$ depends on the virtual time τ.

In this study, we use a semi-implicit fractional-step method [14] to linearize the convection term $(\boldsymbol{c}\cdot\nabla)\psi$ in Eq. (5). Therefore, Eq. (5) is split into two time-discretization equations such as

$$\frac{\psi^{(*)}-\psi^{(k)}}{\Delta\tau}+\left(\boldsymbol{c}^{(k)}\cdot\nabla\right)\psi^{(*)}-\nabla\cdot\left(\varepsilon\nabla\psi^{(*)}\right)=0 \qquad \text{in } \mathcal{D}\times\left[\tau^{(k)},\tau^{(k+1)}\right] \tag{7}$$

$$\frac{\psi^{(k+1)}-\psi^{(*)}}{\Delta\tau}=\mathcal{s}(\phi) \qquad \text{in } \mathcal{D}\times\left[\tau^{(k)},\tau^{(k+1)}\right] \tag{8}$$

where $\Delta\tau$ is the incremental virtual time-step; $\psi^{(k)}$ and $\psi^{(k+1)}$ are the LS values at virtual time $\tau^{(k)}$ and $\tau^{(k+1)}$, respectively; $\psi^{(*)}$ are one intermediate LS value at $\tau^{(*)}\in\left[\tau^{(k)},\tau^{(k+1)}\right]$.

3. Polygonal finite element method for level set evolution

3.1. Poly-FEM for conventional level set evolution

3.1.1. Poly-FEM for implicit level set evolution

From strong form in Eq. (3), we assume $\mathbb{Q}^t=\{\phi:\phi(\boldsymbol{x},t)\in\mathbb{H}^1(\mathcal{D}),\ t\in\mathcal{T}\}$ and $\mathbb{W}\in\mathbb{H}^1(\mathcal{D})$ are the space of time-independent trial solution and the space of time-independent test function. By using the integration by parts and the divergence theorem, we can rewrite the weak form (3) into the following compact form: for given $\phi^{(n)}\in\mathbb{Q}^t$, find $\phi^{(n+1)}\in\mathbb{Q}^t$ such that $\forall w\in\mathbb{W}$,

$$\underbrace{\mathcal{A}\left(w,\phi^{(n+1)}\right)}_{\text{Standtard Galerkin}}+\underbrace{\mathcal{B}\left(w,\phi^{(n+1)}\right)}_{\text{Stabilization terms}}=\underbrace{\mathcal{A}\left(w,\phi^{(n)}\right)}_{\text{Standtard Galerkin}}+\underbrace{\mathcal{B}\left(w,\phi^{(n)}\right)}_{\text{Stabilization terms}} \tag{9}$$

with

JTE HCMUTE
ISSN: 2615-9740
JOURNAL OF TECHNICAL EDUCATION SCIENCE
Ho Chi Minh City University of Technology and Education
Website: https://jte.hcmute.edu.vn/index.php/jte/index
Email: jte@hcmute.edu.vn

$$\mathcal{A}\left(w,\phi^{(n+1)}\right)=\int_{\mathcal{D}} w\phi^{(n+1)}\mathrm{d}\mathcal{D}+\frac{\Delta t}{2}\int_{\mathcal{D}} w(\boldsymbol{v}\cdot\nabla)\phi^{(n+1)}\mathrm{d}\mathcal{D}+\frac{\Delta t}{2}\int_{\mathcal{D}} \varepsilon\nabla w\cdot\nabla\phi^{(n+1)}\mathrm{d}\mathcal{D} \quad (10)$$

$$\mathcal{A}\left(w,\phi^{(n)}\right)=\int_{\mathcal{D}} w\phi^{(n)}\mathrm{d}\mathcal{D}-\frac{\Delta t}{2}\int_{\mathcal{D}} w(\boldsymbol{v}\cdot\nabla)\phi^{(n)}\mathrm{d}\mathcal{D}-\frac{\Delta t}{2}\int_{\mathcal{D}} \varepsilon\nabla w\cdot\nabla\phi^{(n)}\mathrm{d}\mathcal{D} \quad (11)$$

$$\mathcal{B}\left(w,\phi^{(n+1)}\right)=\frac{\Delta t}{2}\int_{\mathcal{D}} \phi^{(n+1)}(\boldsymbol{v}\cdot\nabla)w\mathrm{d}\mathcal{D}+\frac{\varepsilon\Delta t}{2}\int_{\mathcal{D}} \nabla\phi^{(n+1)}\cdot\nabla w\mathrm{d}\mathcal{D}+\left(\frac{\Delta t}{2}\right)^2\int_{\mathcal{D}}(\boldsymbol{v}\cdot\nabla)w(\boldsymbol{v}\cdot\nabla)\phi^{(n+1)}\mathrm{d}\mathcal{D} \quad (12)$$

$$\mathcal{B}\left(w,\phi^{(n)}\right)=\frac{\Delta t}{2}\int_{\mathcal{D}} \phi^{(n)}(\boldsymbol{v}\cdot\nabla)w\mathrm{d}\mathcal{D}+\frac{\varepsilon\Delta t}{2}\int_{\mathcal{D}} \nabla\phi^{(n)}\cdot\nabla w\mathrm{d}\mathcal{D}-\left(\frac{\Delta t}{2}\right)^2\int_{\mathcal{D}}(\boldsymbol{v}\cdot\nabla)w(\boldsymbol{v}\cdot\nabla)\phi^{(n)}\mathrm{d}\mathcal{D} \quad (13)$$

where Δt is the incremental time-step, $\phi^{(n)}$ and $\phi^{(n+1)}$ are the LS values at time $t^{(n)}=\left(t^{(0)}+n\Delta t\right)$ and $t^{(n+1)}=\left(t^{(n)}+\Delta t\right)$, respectively.

3.1.2. Poly-FEM for re-initialization process

Similar as sub-section above, we also apply the standard least-square method for the spatial discretization of Eq. (7). Meanwhile, the standard Galerkin method is applied for the simple problem in Eq. (8). Consequently, the weak formulation of Eqs. (7) and (8) can be written into the following compact form: for given $\psi^{(k)}$, find $\left\{\psi^{(*)},\psi^{(k+1)}\right\}\in\mathbb{Q}^{\tau}:=\{\psi:\psi(\boldsymbol{x},\tau)\in\mathbb{H}^1(\mathcal{D}),\ \tau\in\mathcal{T}_{\tau}\}$ such that $\forall w\in\mathbb{W}$

$$\underbrace{\mathcal{A}_{\tau}\left(w,\psi^{(*)}\right)}_{\text{Stand. Galerkin}}+\underbrace{\mathcal{B}_{\tau}\left(w,\psi^{(*)}\right)}_{\text{Stab. terms}}=\underbrace{\mathcal{A}_{\tau}\left(w,\psi^{(k)}\right)}_{\text{Stand. Galerkin}}+\underbrace{\mathcal{B}_{\tau}\left(w,\psi^{(k)}\right)}_{\text{Stab. term}} \quad (14)$$

$$\int_{\mathcal{D}} w\psi^{(k+1)}\mathrm{d}\mathcal{D}=\int_{\mathcal{D}} w\psi^{(*)}\mathrm{d}\mathcal{D}+\Delta\tau\int_{\mathcal{D}} w\mathcal{s}(\phi)\mathrm{d}\mathcal{D} \quad (15)$$

with

$$\mathcal{A}_{\tau}\left(w,\psi^{(*)}\right)=\int_{\mathcal{D}} w\psi^{(*)}\mathrm{d}\mathcal{D}+\Delta\tau\int_{\mathcal{D}} w\boldsymbol{c}^{(k)}\nabla\psi^{(*)}\mathrm{d}\mathcal{D}+\Delta\tau\int_{\mathcal{D}} \varepsilon\nabla w\cdot\nabla\psi^{(*)}\mathrm{d}\mathcal{D} \quad (16)$$

$$\mathcal{A}_{\tau}\left(w,\psi^{(k)}\right)=\int_{\mathcal{D}} w\psi^{(k)}\mathrm{d}\mathcal{D} \quad (17)$$

$$\mathcal{B}_{\tau}\left(w,\psi^{(*)}\right)=\Delta\tau\int_{\mathcal{D}} \psi^{(*)}\boldsymbol{c}^{(k)}\nabla w\mathrm{d}\mathcal{D}+\Delta\tau\int_{\mathcal{D}} \varepsilon\nabla\psi^{(*)}\cdot\nabla w\mathrm{d}\mathcal{D}+\Delta\tau^2\int_{\mathcal{D}}\left(\boldsymbol{c}^{(k)}\nabla w\right)\left(\boldsymbol{c}^{(k)}\nabla\psi^{(*)}\right)\mathrm{d}\mathcal{D} \quad (18)$$

$$\mathcal{B}_{\tau}\left(w,\psi^{(k)}\right)=\Delta\tau\int_{\mathcal{D}} \psi^{(k)}\boldsymbol{c}^{(k)}\nabla\varphi\mathrm{d}\mathcal{D}+\Delta\tau\int_{\mathcal{D}} \varepsilon\nabla\psi^{(k)}\cdot\nabla w\mathrm{d}\mathcal{D} \quad (19)$$

3.2. Shape functions on arbitrary polygonal elements

(a) *(b)*

Figure 2. *Wachspress shape functions for polygonal element: (a) Definition of Wachspress coordinates; (b) Wachspress shape function*

JTE HCMUTE
ISSN: 2615-9740
JOURNAL OF TECHNICAL EDUCATION SCIENCE
Ho Chi Minh City University of Technology and Education
Website: https://jte.hcmute.edu.vn/index.php/jte/index
Email: jte@hcmute.edu.vn

In Poly-FEM framework, we assume that $\Omega \subset \mathbb{R}^2$ has been partitioned into n_e non-overlapping polygonal elements Ω^e involving n_s edges and n_n nodes such that $\Omega \approx \Omega^h := \sum_{e=1}^{n_e} \Omega^e$. For each polygonal element Ω^e, we will denote with vertices $\boldsymbol{x}_1, \boldsymbol{x}_2, \dots, \boldsymbol{x}_{n_{ne}}, n_{ne} \geq 3$ in counter-clockwise ordering. For any point $\boldsymbol{v} \in \Omega^e$, let $h_i(\boldsymbol{x})$ denote the perpendicular distance of $\boldsymbol{v}$ to the edge $\boldsymbol{e}_i$, as shown in Figure 2a. We define $\boldsymbol{p}_i(\boldsymbol{x}) = \boldsymbol{n}_i / h_i(\boldsymbol{x})$, where $\boldsymbol{n}_i$ is the outward unit normal vector to the edge $\boldsymbol{e}_i = [\boldsymbol{x}_i, \boldsymbol{x}_{i+1}]$, with vertices indexed cyclically $\boldsymbol{x}_{n_{ne}+1} = \boldsymbol{x}_1$. Then the Wachspress shape functions and their gradients are expressed as [15]

$$N_i(\boldsymbol{x}) = \frac{\widetilde{w}_i(\boldsymbol{x})}{\sum_{j=1}^{n} \widetilde{w}_j(\boldsymbol{x})} \quad \text{with} \quad \widetilde{w}_i = \det(\boldsymbol{p}_{i-1}, \boldsymbol{p}_i) \tag{20}$$

$$\nabla N_i = N_i\left(\boldsymbol{\mathcal{R}}_i - \sum_{j=1}^{n} N_j \boldsymbol{\mathcal{R}}_j\right) \quad \text{with} \quad \boldsymbol{\mathcal{R}}_i = \boldsymbol{p}_{i-1} + \boldsymbol{p}_i \tag{21}$$

Figure 2b illustrates the Wachspress shape function of a regular polygonal element.

4. Numerical investigations

In this section, two benchmark problems are investigated to show the effective of the present method in solving LS equations. The value of the viscosity coefficient ε is 10^{-3} both the unsteady LS convection-diffusion transport (3) and the Eikonal equation (5) for a rigid body rotation of Zalesak's disk, and a time-reversed single-vortex flow problem. The re-initialization process is performed after each 5 iterations of the interface evolution process. In the re-initialization process, the LS function is reinitialized after every iteration of the shape evolution by solving 5 virtual time steps.

4.1. Rigid body rotation of Zalesak's disk

A benchmark rigid body rotation of Zalesak's disk is considered as the first example. In this example, a slotted disk is centered at $(50, 75)$ in a 100×100 domain with a radius of 15, a length of 25, and a width of 5. The disk rotates counter-clockwise around the center point $(50, 50)$ by the action of a velocity field. The velocity field is given by

$$\begin{cases} u = (\pi/314)(50 - y) \\ v = (\pi/314)(x - 50) \end{cases} \tag{22}$$

The disk completes one evolution and returns to the initial position after every 628 time units. We can identify dissipation and dispersion errors of the interface by the following error equation

$$\text{Error} = \sqrt{\frac{\sum_{|\phi|<\varepsilon} (\phi_{\text{num}} - \phi_{\text{exact}})^2}{M}} \tag{23}$$

where M is the number of nodes at near the interface where the absolute value of ϕ is less than $\varepsilon = 2h$ (h is the element size). The change of the error which is defined by Eq. (23) according to the element size of T3, Q4, and polygonal elements are shown in Figure 3a. As shown in this figure, the errors of polygonal elements are smaller than T3 and Q4 elements for fine mesh. In addition, in order to check the area conservation of the proposed method, we also consider the absolute relative area error (%), and this error is given by

$$\varepsilon_M = \left|\frac{A_f - A_i}{A_i}\right| \cdot 100 \tag{24}$$

where $A_f = \int_\Omega H(\phi) \mathrm{d}\Omega$ is the total area of the slotted disk after one rotation, A_i is the total area of the initial slotted disk, and $H(\phi)$ is a Heaviside function defined by

$$H(\phi) = \begin{cases} 0 & \text{if} \quad \phi < -\varepsilon \\ \frac{1}{2}\left[1 + \frac{\phi}{\varepsilon} + \frac{1}{\pi}\sin\left(\frac{\pi\phi}{\varepsilon}\right)\right] & \text{if} \quad |\phi| \leq \varepsilon \\ 1 & \text{if} \quad \phi > \varepsilon \end{cases} \tag{25}$$

JTE
HCMUTE
ISSN: 2615-9740

JOURNAL OF TECHNICAL EDUCATION SCIENCE
Ho Chi Minh City University of Technology and Education
Website: https://jte.hcmute.edu.vn/index.php/jte/index
Email: jte@hcmute.edu.vn

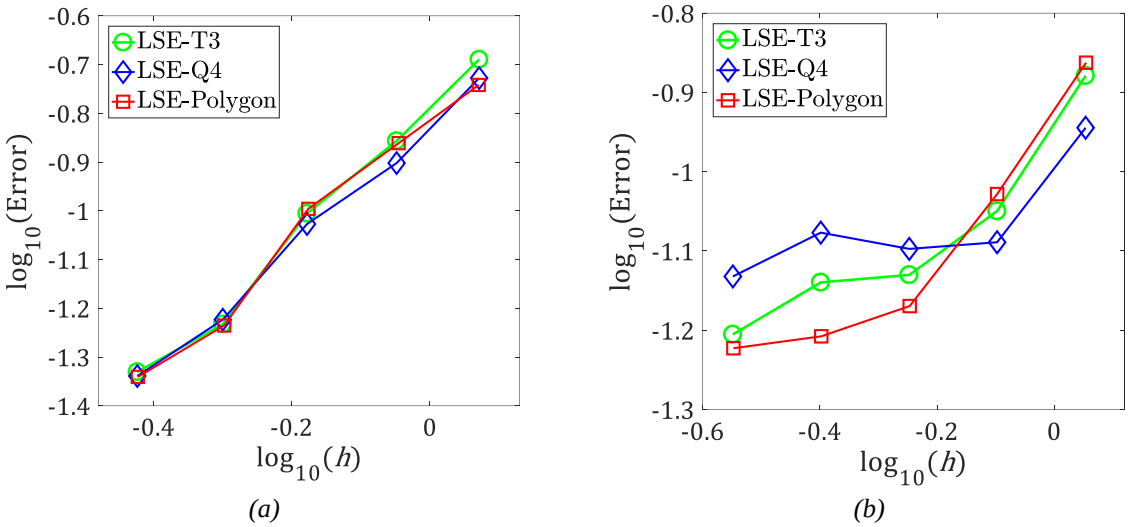

Figure 3. *Plots of the error follows the element size: (a) rigid body rotation of Zalesak's disk problem; (b) a time-reversed single-vortex problem*

where ε is set to $2h$ (h is the element size). A comparison of the absolute relative area errors between T3, Q4, and polygonal elements for the problem of Zalesak's disk rotation is performed in Table 1. As shown in Table 1, the polygonal elements are better area conservation than T3, Q4 elements for the same element size.

Table 1. *Comparison of the absolute relative area errors (%) between T3, Q4, and polygonal elements for the problem of Zalesak's disk rotation*

Element size	T3	Q4	Polygon
1.1768	0.4909	0.7169	0.5032
0.9011	0.4439	0.6129	0.2919
0.6668	0.0965	0.1037	0.0621
0.5038	0.1327	0.1986	0.1702
0.3778	0.1164	0.1430	0.1006

In this example, we also investigate the shapes of the slotted disk at $t = 628$s for the LSE method on the T3, Q4, and polygonal mesh with approximately the same element size as shown in Figure 4. Note that the LSE method may lead to a misleading accuracy of area error due to fortuitous cancellation of inward (negative) and outward (positive) dissipation errors when only area conservation is considered [5]. Especially, we also see that the shape of the slotted disk uses polygonal elements which is the closest similarity to the initial shape.

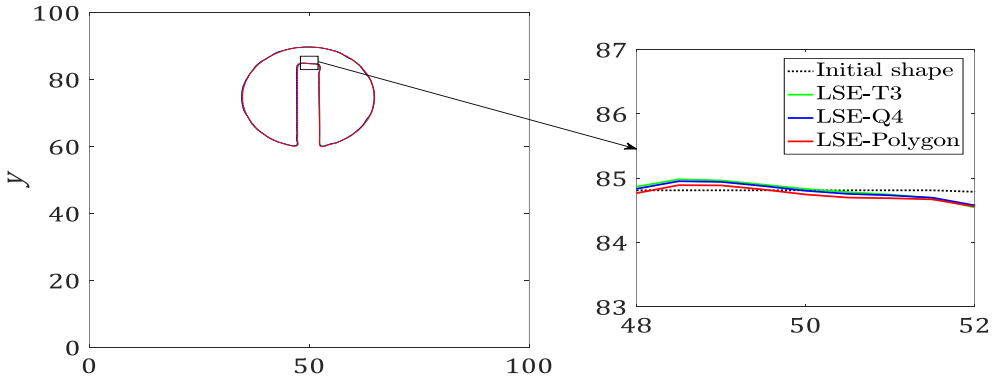

Figure 4. *The shapes of the slotted disk at $t = 628s$ for the LSE method by using T3, Q4, and polygonal elements with approximately the same element size*

JTE
HCMUTE
ISSN: 2615-9740

JOURNAL OF TECHNICAL EDUCATION SCIENCE
Ho Chi Minh City University of Technology and Education
Website: https://jte.hcmute.edu.vn/index.php/jte/index
Email: jte@hcmute.edu.vn

4.2. Simulation of a time-reversed single-vortex problem

The second example is the problem of a time-reversed single-vortex flow. In this example, a circular fluid is centered at $(50, 75)$ in a 100×100 domain with a radius of 15, and it is acted by a velocity field

$$\begin{cases} u = -\sin^2(\pi x/100) \cdot \sin(\pi y/50) \cdot \cos(\pi t/T) \\ v = \sin(\pi x/50) \cdot \sin^2(\pi y/100) \cdot \cos(\pi t/T) \end{cases} \quad (26)$$

where $T = 800$ is the time in which the single-vortex returns its initial circular shape. We can define dissipation and dispersion errors of the interface by the following error equation

$$\text{Error} = \sqrt{\frac{\sum_{|\phi|<\varepsilon}\{(\phi_{\text{num}} - \phi_{\text{exact}})/R\}^2}{M}} \quad (27)$$

where R is the radius of the circular fluid element. The change of the error that defined by Eq. (27) follows the element size of T3, Q4, and polygonal elements are shown in Figure 3b. As shown in this figure, the polygonal elements give the better solution than the T3 and Q4 for the fine mesh. Besides, the evolution of the single-vortex over time is also investigated. Figure 5 shows the evolution of the single-vortex at $t = 200, 400, 600,$ and $800s$ for LSE method on a polygonal mesh with the element size of 0.2834. As shown in this figure, we see that the initial circular fluid element almost remains its initial shape after a cycle with T of $800s$.

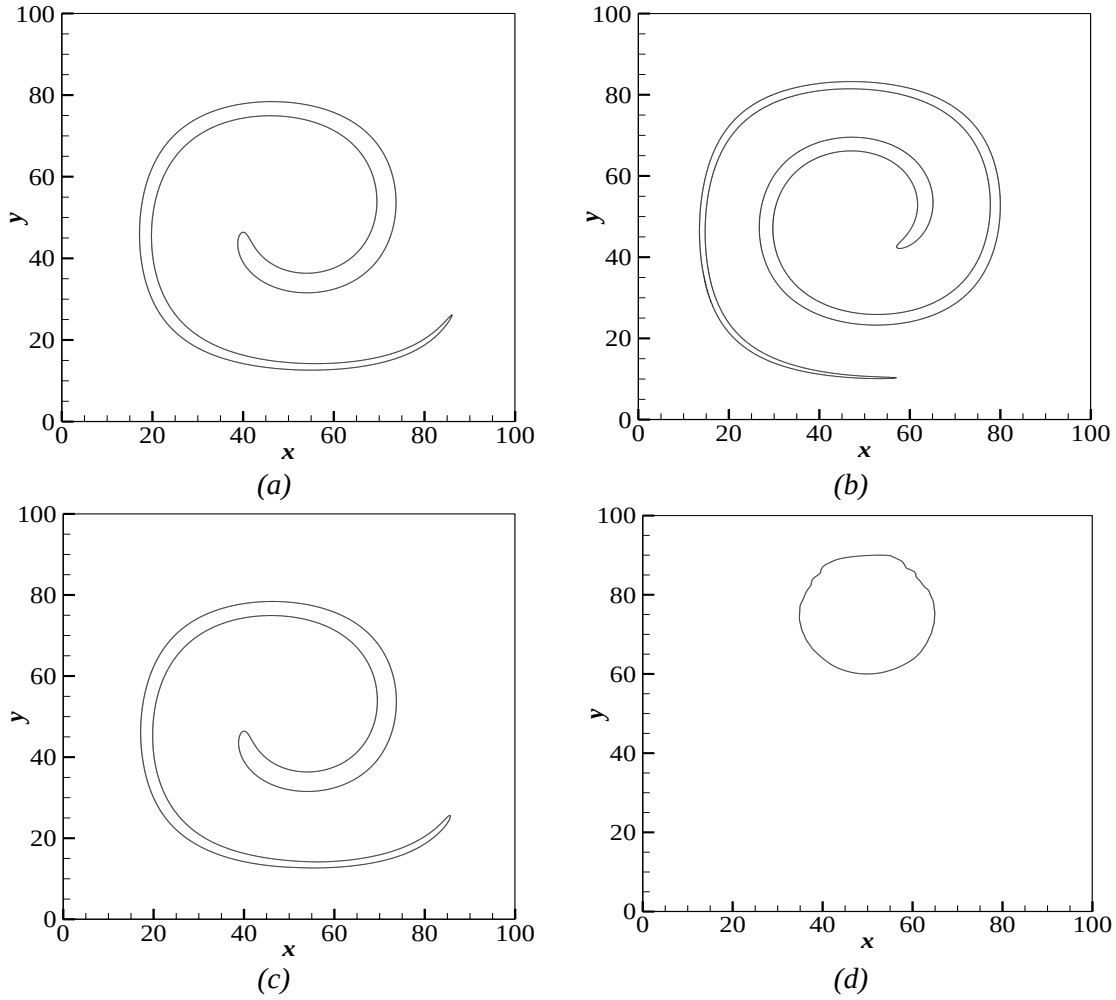

Figure 5. *The evolution of the single-vortex follows the time for LSE method on a polygonal mesh with the element size of* 0.2834*: (a)* $t = 200s$ $(T/4)$*; (b)* $t = 400s$ $(T/2)$*; (c)* $t = 600s$ $(3T/4)$*; (d)* $t = 800s$ (T)

In this example, we also compare the absolute relative area errors of the present study with the previously published studies as shown in Table 2. Table 2 shows that the present results completely match the previously published results.

Table 2. *Comparison of the absolute relative area errors (%) in the present study with the previously published studies*

Element size	Present	Particle LSM [16]	Hybrid particle LSM [17]	LSM [17]
2.2668	11.046	17.9	1.8	100
1.1334	2.422	4.2	0.7	39.8
0.5667	2.408	2.1	0.4	10.3
0.2834	0.264	-	-	-

5. Conclusions

This paper applies an artificial viscosity method to convert an unsteady level set (LS) convection equation into an unsteady LS convection-diffusion transport equation to stabilize the numerical solution of the convection term. Thereafter, a novel least-square polygonal finite element method is used to solve an unsteady LS convection-diffusion problem. Besides, the Wachspress coordinates is used with iso-parametric mapping on a reference element to construct conforming approximations on meshing structures.

The proposed method is evaluated numerically in two different benchmark problems: a rigid body rotation of Zalesak's disk, and a time-reversed single-vortex flow. The results show that in comparison with T3 and Q4 elements, polygonal elements provide a great flexibility in mesh design for arbitrary complex-shaped models in solving the LS equations. Especially, the polygonal elements give the better solution than the T3 and Q4 for the fine mesh. In addition, the numerical results are also compared with the results which obtained from essentially non-oscillatory type formulations and particle LS methods. The results show that the proposed method completely matches the previously published results.

In the future, the proposed method can extend for 3D model as well as the different problems of engineering structures.

REFERENCES

[1] S.H. Nguyen and H.-G. Kim, "Stress-constrained shape and topology optimization with the level set method using trimmed hexahedral meshes," *Methods Appl. Mech. Engrg.*, vol. 366, pp. 061-113, 2020.
[2] C. Basting, D. Kuzmin, "A minimization-based finite element formulation for interface-preserving level set reinitialization," *Computing*, vol. 95, no. 1, pp. 13-25, 2012.
[3] S. Osher and R. Fedkiw, *Level Set Methods and Dynamic Implicit Surfaces*, Verlag New York: Springer, 2003.
[4] M. Sussman, P. Smereka, S. Osher, "A level set approach for computing solutions to incompressible two-phase flow," *J. Comput. Phys.*, vol. 144, no. 1, pp. 146-159, 1994.
[5] H.G. Choi, "A least-square weighted residual method for level set simulation," *Int. J. Numer. Meth. Fluids*, vol. 68, pp. 887-904, 2012.
[6] J.A. Sethian, "A fast marching level set method for monotonically advancing fronts," *Proc. Natl. Acad. Sci. USA*, vol. 93, no. 4, pp. 1591-1595, 1996.
[7] R.N. Elias, M.A.D. Martins, and A.L.G.A. Coutinho, "Simple finite element-based computation of distance functions in unstructured grids," *Int. J. Numer. Methods Engrg*, vol. 72, pp. 1095-1110, 2007.
[8] H. N.-Xuan, S. N.-Hoang, T. Rabczuk, and K. Hackl, "A polytree-based adaptive approach to limit analysis of cracked structures," *Computer Methods in Applied Mechanics and Engineering*, vol. 313, pp. 1006-1039, 2017.
[9] H. N.-Xuan, "A polygonal finite element method for plate analysis," *Computers & Structures*, vol. 188, pp. 45-62, 2017.
[10] T.J. Barth and J.A. Sethian, "Numerical schemes for the Hamilton-Jacobi and level set equations on triangulated domains," *J. Comput. Phys.*, vol. 145, pp. 1-40, 1998.
[11] C. Lin, H. Lee, T. Lee, and L.J. Weber, "A LS characteristic Galerkin finite element method for free surface flows," *Int. J. Numer. Meth. Fluids*, vol. 49, pp. 521-547, 2005.
[12] E. Marchandise, J.-F. Remacle, and N. Chevaugeon, "A quadrature-free discontinuous Galerkin method for the level set equation," *J. Comput. Phys*., vol. 212, pp. 338-357, 2006.
[13] M.H. Cho, H.G. Choi, and J.Y. Yoo, "A direct reinitialization approach of level-set/splitting finite element method for simulating incompressible two-phase flows," *Int. J. Numer. Meth. Fluids*, vol. 67, pp. 1637-1654, 2011.
[14] J. Donea and A. Huerta, Finite element methods for flow problems, Chichester: Wiley, 2003.
[15] M.S. Floater, A. Gillette, and N. Sukumar, "Gradient bounds for Wachspress coordinates on polytopes," *SIAM Journal of Numerical Analysis*, vol. 52, no. 1, pp. 515-532, 2014.
[16] S. E. Hieber and P. Koumoutsakos, "A Lagrangian particle level set method," *Journal of Computational Physics.*, vol. 204, no. 1, pp. 342-367, 2005.
[17] D. Enright, R. Fedkiw, J. Ferziger, and I. Mitchell, "A Hybrid Particle Level Set Method for Improved Interface Capturing," *Journal of Computational Physics.*, vol. 183, no. 1, pp. 83-116, 2002.

Ba-Dinh Nguyen-Tran. received the B.S degree in mechanical engineering from Ho Chi Minh City University of Technology and Education, Ho Chi Minh, Viet Nam, in 2017 and the M.S. degree in engineering mechanics from Ho Chi Minh City University of Technology and Education, Ho Chi Minh, Viet Nam, in 2019.
From 2019 to present, he is a staff in Japan Technology and Engineering Co. Ltd, Ho Chi Minh, Viet Nam. His research interest includes: computational mechanics, fluid-Structure interaction.

Son H. Nguyen. is a full-time researcher in Institute for Computational Science at Ton Duc Thang University. His research interests are in the area of computational solid mechanics with a particular emphasis on topology optimization using the level set method and polygonal elements.

Duc-Huynh Phan. received the B.S. degree in aeronautical engineering from HCMC University of Technology, Ho Chi Minh, Viet Nam, in 2001, the M.S. degree in mechanics of constructions from University of Liège, Wallonia, Belgium, in 2003, and the Ph.D. degree in Structural control from Ritsumeikan University, Kyoto, Japan, in 2008.
From 2008 to present, he is a lecturer in HCMC University of Technology and Education, Ho Chi Minh, Viet Nam. His research interest includes: structural stability, computational mechanics, fluid-Structure interaction, and multi-body dynamics.